



# Study on the consistency between field synergy principle and entransy dissipation extremum principle



Zhi-Qiang Yu, Peng Wang, Wen-Jing Zhou, Zeng-Yao Li, Wen-Quan Tao\*

Key Laboratory of Thermo-Fluid Science and Engineering, Ministry of Education, School of Energy and Power Engineering, Xi'an Jiaotong University, Shaanxi 710049, PR China

## ARTICLE INFO

### Article history:

Received 21 July 2017

Received in revised form 5 September 2017

Accepted 11 September 2017

Available online 21 September 2017

### Keywords:

Field synergy number

Field synergy principle

Entransy dissipation extremum principle

Fin-and-tube surfaces

Composite porous materials

Fluid flow and heat transfer characteristics

## ABSTRACT

This paper is aiming at numerically demonstrating the interrelationship and consistency between field synergy principle (FSP) via the field synergy number (Fc) and the entransy dissipation extremum principle (EDEP). Numerical simulation is conducted by using the FLUENT software and the user defined function programs (UDF) for fin-and-tube surfaces (plain plate and slotted fins) and composite porous materials. The thermal boundary conditions include given heat flux and given surface temperature. The flow includes laminar and turbulent. The air properties may be constant or vary with temperature. Based on the numerical data the analyzed results from the FSP via Fc are totally consistent with the results analyzed by the EDEP for all the cases studied. Such consistency between the FSP and the entransy theory can be regarded as a kind of demonstration of the reliability and correctness of both the FSP and the entransy theory.

© 2017 Elsevier Ltd. All rights reserved.

## 1. Introduction

The efficient utilization of energy is an important subject of researchers around the world. In all the process of natural energy utilization, about 80% involves thermal energy transmission. So, the efficiency of the thermal energy transmission plays an important role in determining the efficiency of the energy utilization.

In past decades, many enhancement technologies and physical mechanisms for improving heat transfer performance have been proposed and applied, such as constructing fin and ribs, imposing mechanical vibration, appending electromagnetic field, developing secondary flow and increasing turbulence intensity. However, as indicated in [1] there was lack of general theoretical analysis and guidance in the enhancing heat transfer process up to the end of last century.

In 1998, based on the energy equation of convective heat transfer, Guo et al. [2–5] proposed field synergy principle (FSP) for revealing the basic mechanism of enhancing convective heat transfer. For the reader's convenience, the major analysis processes of [2–5] are described as follows. For two-dimensional laminar boundary layer, the energy equation of convective heat transfer can be shown as

$$\rho c_p \left( u \frac{\partial T}{\partial x} + v \frac{\partial T}{\partial y} \right) = \frac{\partial}{\partial y} \left( \lambda \frac{\partial T}{\partial y} \right) \quad (1)$$

Integrating Eq. (1) along the thermal boundary thickness and noting that at the outer boundary the fluid temperature gradient equals zero, yields:

$$\int_0^{\delta_t} \rho c_p \left( u \frac{\partial T}{\partial x} + v \frac{\partial T}{\partial y} \right) dy = -\lambda \frac{\partial T}{\partial y} \Big|_w \quad (2)$$

where  $\delta_t$  is the thermal boundary layer thickness. Noting that

$$u \frac{\partial T}{\partial x} + v \frac{\partial T}{\partial y} = \vec{U} \cdot \nabla T \quad (3)$$

Following equation can be obtained:

$$\int_0^{\delta_t} \rho c_p (\vec{U} \cdot \nabla T) dy = -\lambda \frac{\partial T}{\partial y} \Big|_w \quad (4)$$

Through non-dimensional treatment, Eq. (4) can be transformed into

$$Nu_x = Re_x Pr \int_0^1 (\vec{U} \cdot \nabla \bar{T}) d\bar{y} = Re_x Pr \int_0^1 (|\vec{U}| \cdot |\nabla \bar{T}| \cdot \cos \theta) d\bar{y} \quad (5)$$

where  $\vec{U} = U/U_\infty$ ,  $\nabla \bar{T} = \nabla T / [(T_\infty - T_w) / \delta_t]$ ,  $\bar{y} = y / \delta$ ,  $T_\infty > T_w$ , and  $\theta$  is the angle between velocity vector and temperature gradient (synergy angle).

Eqs. (4) or (5) is the math expression of the field synergy principle (FSP) which indicates that the intensity of heat transfer depends not only on the temperature difference between flow fluid and solid wall, flow velocity, but also on the intersection angle between velocity vector and fluid temperature gradient. There

\* Corresponding author.

E-mail address: [wqtao@mail.xjtu.edu.cn](mailto:wqtao@mail.xjtu.edu.cn) (W.-Q. Tao).



tion for which the synergy number should be one ( $F_c = 1$ ) or the averaged synergy angle should be zero (fluid heated) or  $180^\circ$  (fluid cooled). In [43,44] the consistency between FSP and EDEP was investigated from the view point of synergy angle for several examples including both laminar and turbulent flow, while in the present paper it will be studied from view point of field synergy number. In [42] the authors adopted the variational relations of the entransy dissipation and the field synergy degree with the laminar heat transfer performance, and some comparisons were made between FSP and that of the EDEP. Their results show that, for given temperature boundary conditions, both FSP and EDEP can lead to maximizing the total heat flow rate. However, for given heat flux boundary conditions, only the optimization equation based on the EDEP intends to minimize the heat transfer temperature difference, while the optimization based on the FSP makes no sense. It is the present authors' consideration that for the given wall heat flux cases the integration of object function in their variational function is the heat flux which has been specified constant. Thus no role can be played by FSP. If we discuss from another view point, that is for the given wall heat flux boundary condition we solicit for the minimum temperature difference between wall and fluids, both FSP and EDEP can play a role and the results are expected to be in consistency, as this has been demonstrated in [43,44] from the view point of synergy angle.

As indicated above this paper adopts the field synergy number and applies it to analyze and evaluate the performance of heat transfer. Through the field synergy number, the connection between the FSP and EDEP is analyzed deeply via eight numerical examples, including plain plate fin-an-tube surface, slotted fin-and-tube surfaces, and six structures of composite porous materials. The given thermal boundary conditions are constant heat flux and constant wall temperature. The flow includes laminar flow and turbulent flow. The fluid property covers both constant property and variable property. From the numerical results and analysis, the connection between FSP and EDEP is discussed and obtained through the field synergy number and their inherently consistent feature is very definitely demonstrated.

In the following presentation, the field synergy number will first be introduced and its general expression for complicated connective heat transfer case will be derived in Section 2. In Section 3 numerical simulation models and numerical methods will be briefly presented. In Section 4 numerical results for the two fin-and-tube surfaces will be presented and connection between FSP and EDEP is discussed. The results and analysis for the six porous structures will be conducted in Section 4. Finally some conclusions are drawn in Section 5.

## 2. Field synergy number and its general computation formula

Guo et al. defined the field synergy number as follows [4]

$$F_c = \frac{Nu}{RePr} \tag{6}$$

For fluid flow and heat transfer over a flat plate they obtained:

$$F_c = \frac{Nu}{RePr} = \int_0^{\delta^*} \int \bar{U} \cdot \nabla \bar{T} d\bar{y} \tag{7}$$

Here,  $F_c$  represents the synergy degree between velocity vector and fluid temperature gradient of the entire domain. As indicated by Li and Guo [5] that for most practical convective heat transfer situations their synergy number are much less than one, indicating great rooms for enhancement study.

In the following a general expression of the field synergy number will be derived for convective heat transfer within a complicated region as shown in Fig. 1. For the steady turbulent fluid

flow and heat transfer without inner source in a complicated region shown in Fig. 1, neglecting the viscous dissipation term, the energy equation is

$$U \cdot \nabla(\rho c_p T) = \nabla(\lambda \nabla T) \tag{8}$$

By integrating Eq. (8) over the heat transfer region shown in Fig. 1 and adopting Gauss formula, we have:

$$\iiint_V [U \cdot \nabla(\rho c_p T)] dV = \iint_S (\lambda \nabla T) d\vec{S} \tag{9}$$

where  $V$  is the volume of the studied region and  $S$  is its boundary. Neglecting the diffusion in fluids the boundary integration of the right hand of Eq. (9) is the heat transfer rate between fluid and solid wall, and adopting the Newton's law of cooling we have

$$h(T_{wm} - T_{fm})S = \iiint_V [U \cdot \nabla(\rho c_p T)] dV \tag{10}$$

Introducing the characteristic length  $D$  ( $D = \frac{4V}{S}$ ) and following dimensionless variables:

$$d\bar{V} = \frac{dV}{V}, \quad \bar{U} = \frac{U}{U_m}, \quad \bar{T} = \frac{T}{(T_{wm} - T_{fm})/D}, \quad \bar{\rho} = \frac{\rho}{\rho_m}, \quad \bar{c}_p = \frac{c_p}{c_{pm}}$$

where the subscript  $m$  stands for the mean values of the fluid or solid. By some management we have:

$$Q_s = h(T_{wm} - T_{fm})S = \frac{\rho_m c_{pm} U_m (T_{wm} - T_{fm}) S}{4} \iiint_V [\bar{U} \cdot \nabla(\bar{\rho} \bar{c}_p \bar{T})] d\bar{V} \tag{11}$$

$$\text{Then, } \frac{1}{4} \iiint_V [\bar{U} \cdot \nabla(\bar{\rho} \bar{c}_p \bar{T})] d\bar{V} = \frac{Q_s}{\rho_m c_{pm} U_m (T_{wm} - T_{fm}) S} \tag{12}$$

$$h = \frac{\rho_m c_{pm} U_m}{4} \iiint_V [\bar{U} \cdot \nabla(\bar{\rho} \bar{c}_p \bar{T})] d\bar{V} \tag{13}$$

$$\text{i.e., } Nu = \frac{1}{4} RePr \iiint_V [\bar{U} \cdot \nabla(\bar{\rho} \bar{c}_p \bar{T})] d\bar{V} \tag{14}$$

According to the definition of field synergy number, Eq. (6), we have

$$F_c = \frac{Nu}{RePr} = \frac{1}{4} \iiint_V [\bar{U} \cdot \nabla(\bar{\rho} \bar{c}_p \bar{T})] d\bar{V} = \frac{Q_s}{\rho_m c_{pm} U_m (T_{wm} - T_{fm}) S} \tag{15}$$

$$Nu = \frac{1}{4} RePr \iiint_V [\bar{U} \cdot \nabla(\bar{\rho} \bar{c}_p \bar{T})] d\bar{V} = RePr \frac{Q_s}{\rho_m c_{pm} U_m (T_{wm} - T_{fm}) S} \tag{16}$$

Eqs. (15) and (16) show that from numerical simulation results, such as  $Q_s$ ,  $T_{wm}$ , etc., the correspondent values of  $F_c$  and  $Nu$  can be obtained with ease. And the value of  $F_c$  is taken as the indicator of

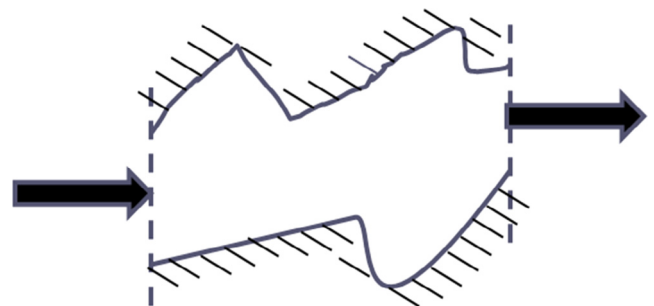


Fig. 1. Convective heat transfer within a complicated region.

synergy between velocity vector and fluid temperature gradient of the entire heat transfer domain.

In the field synergy principle, the field synergy angle refers to the angle between velocity vector and temperature gradient vector to evaluate the local synergy degree. The local weak place in the heat transfer process can be found out through the local field synergy angle. So, the heat transfer performance can be improved by setting up enhancing structures such as slots on the weak place and so on. As for the field synergy number, it is applied to analyze and evaluate the heat transfer performance from the point of global view. As it can be observed from Eq. (15), the value of  $F_c$  is actually the volume integration of the dot product of the fluid velocity and the temperature gradient, which has the inherent relationship with the domain integration mean synergy angle defined by [38]:

$$\vartheta_m = \arccos \frac{\sum |\vec{U}_i \cdot \nabla T_i \cos \vartheta_i dV_i}{\sum |\vec{U}_i \cdot \nabla T_i dV_i} \quad (17)$$

Thus the field synergy number reexamines the synergy between velocity vector and fluid temperature gradient for the entire domain, and it is inherently consistent with the field synergy angle.

In the following the consistency between FSP (via field synergy number) and EDEP is analyzed for the two typical boundary conditions:

(1) For given heat flux boundary condition

In the FSP, when giving heat flux boundary condition, then from  $F_c = q_s / [\rho c_p U (T_w - T_a)]$  and  $Nu = Re Pr q_s / [\rho c_p U (T_w - T_a)]$ , it can be seen that if the heat transfer performance is the best the field synergy number should be the maximum and the temperature difference should be the minimum.

In the EDEP, when giving heat flux boundary condition, according to the MinEDP if the heat transfer capability is the strongest the entransy dissipation should be the minimum and the temperature difference should be also minimum.

(2) For given temperature difference boundary condition

In the FSP, when giving temperature difference boundary condition, from  $F_c = q_s / [\rho c_p U (T_w - T_a)]$  and  $Nu = Re Pr q_s / [\rho c_p U (T_w - T_a)]$ , it can be seen that if the heat transfer is the best then the field synergy number should be the maximum, and the heat flux should be the maximum.

In the EDEP, when giving temperature difference boundary condition, according to the MaxEDP if the heat transfer is the strongest then the entransy dissipation should be the maximum and the heat flux should be also maximum.

Above analysis reveals the inherent consistence between the FSP (via  $F_c$ ) and EDEP.

For the comparison purpose we need to select some indicators for EDEP. Here we take the same practice as we adopted in [44]. It is briefly described as follow. For the given boundary heat flux condition, MinEDP says that for the optimum situation the temperature difference and the entransy dissipation should be the minimum [5]. Thus we take temperature difference between wall and fluid,  $\Delta T_m$ , and entransy dissipation,  $\Delta e$ , as the indicators. Obviously, the smaller the  $\Delta T_m$  and  $\Delta e$ , the better the heat transfer process. For the given wall temperature condition, MaxEDP says when the entransy dissipation is the maximum the heat transfer rate will be the maximum. Since for this condition the fluid outlet temperature is the process result and cannot be specified in advance, we take heat flux,  $q_p$ , and the entransy dissipation,  $\Delta e_p$ , for 1 K temperature difference between wall and fluid as the

indicators. Obviously for this situation the larger the dissipation and heat flux the better the process. In addition for the both boundary conditions we also take the equivalent thermal resistance [25],  $R_E$ , as the indicator for which the smaller the value the better the process.

For the reader's convenience all the parameters used in the following presentation are briefly summarized as follows:

$$\theta_i = \cos^{-1} \frac{u_i \frac{\partial T_{ai}}{\partial x} + v_i \frac{\partial T_{ai}}{\partial y} + w_i \frac{\partial T_{ai}}{\partial z}}{|\vec{U}_i| |\nabla T_{ai}|} \quad (18)$$

$$\theta = \frac{\sum \theta_i dV_i}{\sum dV_i} \quad (19)$$

$$Nu = \frac{hl}{\lambda} \quad (20)$$

$$h = \frac{Q}{\Delta T_m A_{tr}} \quad (21)$$

$$Re = \frac{ul}{\nu} = \frac{\rho ul}{\eta} \quad (22)$$

$$Re_{in} = \frac{u_{in} l}{\nu} = \frac{\rho u_{in} l}{\eta} \quad (23)$$

$$Pr = \frac{\nu}{\lambda / \rho c_p} = \frac{\nu}{a} \quad (24)$$

$$F_c = \frac{Q_s}{\rho c_p U (T_w - T_a) S} = \frac{q_s}{\rho c_p U (T_w - T_a)} \quad (25)$$

$$\Delta E = \Delta T_m \cdot Q \quad (26)$$

$$\Delta T_m^{he} = (\Delta T_{max} - \Delta T_{min}) / \ln(\Delta T_{max} / \Delta T_{min}) \quad (27)$$

$$\Delta T_m^{pm} = \frac{1}{S} \iint_S T_w dS - \frac{1}{V} \iiint_V T_a dV \quad (28)$$

$$\Delta e = \Delta T_m \cdot q \quad (29)$$

$$\Delta T_m = \frac{\Delta E}{Q} \quad (30)$$

$$q_p = \frac{\Delta E}{\Delta T_m \cdot A_{tr} \cdot \Delta T_m} \cdot \Delta T_{mp} \quad (31)$$

$$\Delta e_p = \Delta T_{mp} \cdot q_p \quad (32)$$

$$R_E = \frac{\Delta E \cdot A}{Q^2} \quad (33)$$

$$m = \rho V = \rho u_{in} A_{in} \quad (34)$$

In these formulas, the characteristic length  $l$  is the outside diameter of tube in the fin-and-tube surface (plain plate and slotted fins) and is the equivalent diameter of the tetrakaidecahedron unit in the porous material;  $\Delta T_m^{he}$  is the log-mean temperature difference for the two fin-and-tube surfaces,  $\Delta T_m^{pm}$  is that for the porous material.

### 3. Physical models and numerical methods

In this paper three types of convective heat transfer configurations will be introduced for which numerical simulation will be conducted and the relationship between FSP (via field synergy

number) and EDEP will be searched for. These three types of configurations are plain plate and slotted fins, type 1 porous material composed of tetrakaidecahedron units with two equivalent diameters, and type 2 porous material composed of tetrakaidecahedron units with three equivalent diameters. In this section the geometrical parameters of the three configurations and the major features of their numerical treatments will be presented. The numerical results will be provided in the next section.

3.1. Physical models of the plain plate and slotted fins

Two types of fin-and-tube heat transfer surfaces are examined: the plain plate fin and slotted fin, which are shown in Fig. 2 [17].

Because of symmetry and periodic characteristics of the two fin-and-tube surfaces, only the region shown by the dashed lines in Fig. 3 is taken as the computational domain, where the boundary conditions of the six boundaries are also indicated. It should be noted that ahead and behind of the fin region extensions are adopted in order that uniform velocity inlet and outflow condition can be adopted for the inlet and outlet boundaries. The extension times are 1 and 5 lengths of the fin region for the inlet and outlet, respectively.

The heat transfer medium is air and its physical property parameters are assumed to be constant. The air flow is laminar and in steady state. The tube wall temperature is assumed to be constant ( $T_w = 400$  K). The logarithmic mean temperature difference is adopted as the temperature difference of convective heat transfer coefficient.

3.2. Physical models of type 1 porous material

The tetrakaidecahedron model adopted is shown in Fig. 4. In Fig. 4  $d$  is the equivalent diameter of the tetrakaidecahedron unit,  $L_s$  is the length of cylindrical framework, and  $d_s$  is the diameter of cylindrical framework. Based on the tetrakaidecahedron structure characteristics, the following expressions can be figured out:

$$d = 2.828L_s \tag{35}$$

$$\varepsilon = 1 - \frac{9.425}{8\sqrt{2}} \left(\frac{d_s}{L_s}\right)^2 + \frac{3.33}{8\sqrt{2}} \left(\frac{d_s}{L_s}\right)^3 \tag{36}$$

In the simulation  $d = 2.828$  mm, then  $L_s = d/2.828 = 1$  mm. Two equivalent diameters of the tetrakaidecahedron unit are adopted and two porous models constituted:

- (1) Dense porous model (DPM),  $d_s = 0.5 L_s = 0.5$  mm,  $\varepsilon = 0.8285$ .
- (2) Sparse porous model (SPM),  $d_s = 0.2 L_s = 0.2$  mm,  $\varepsilon = 0.9690$ .

It is assumed that many tetrakaidecahedron units sit side by side in order. Then from the symmetry feature of the porous material structure, the calculation domain is one circulation region in the porous material interior. For the models of both DPM and SPM, the length of three periods is selected as shown in Fig. 5.

Based on the above two porous models, two composite porous materials can be formed: DPM-SPM (D-S) and SPM-DPM (S-D). Both of them belong to type 1.

3.3. Physical models of type 2 porous material

In this type of porous material the same tetrakaidecahedron unit is adopted. However, three equivalent diameters will be taken and three porous models are formed:

- (1) Dense porous model (DPM),  $d_s = 0.6 L_s = 0.6$  mm,  $\varepsilon = 0.7637$ .
- (2) Middle porous model (MPM),  $d_s = 0.4 L_s = 0.4$  mm,  $\varepsilon = 0.8855$ .
- (3) Sparse porous model (SPM),  $d_s = 0.2 L_s = 0.2$  mm,  $\varepsilon = 0.9690$ .

Again the length of three periods along the flow direction is selected as the convective heat transfer surface as shown in Fig. 6. Then six composite porous materials can be constituted: DPM-MPM-SPM (D-M-S), DPM-SPM-MPM (D-S-M), MPM-DPM-SPM (M-D-S), MPM-SPM-DPM (M-S-D), SPM-DPM-MPM (S-D-M), SPM-MPM-DPM (S-M-D). All of them belong to type 2 porous material.

For the two types of porous materials, taking D-M-S as an example (see Fig. 7), the boundary conditions of their calculation region

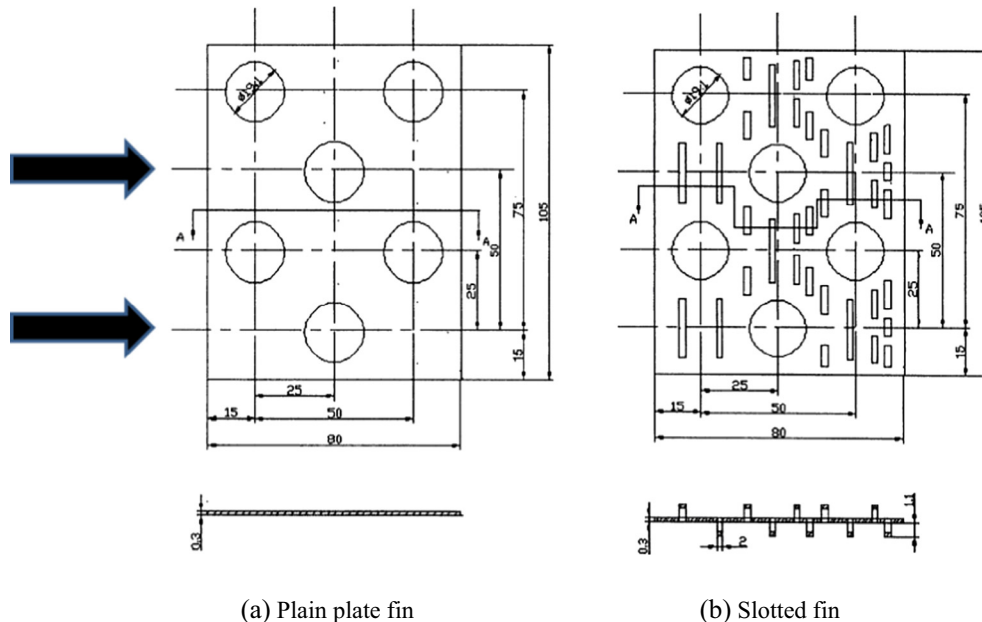


Fig. 2. Plain plate and slotted fins models.

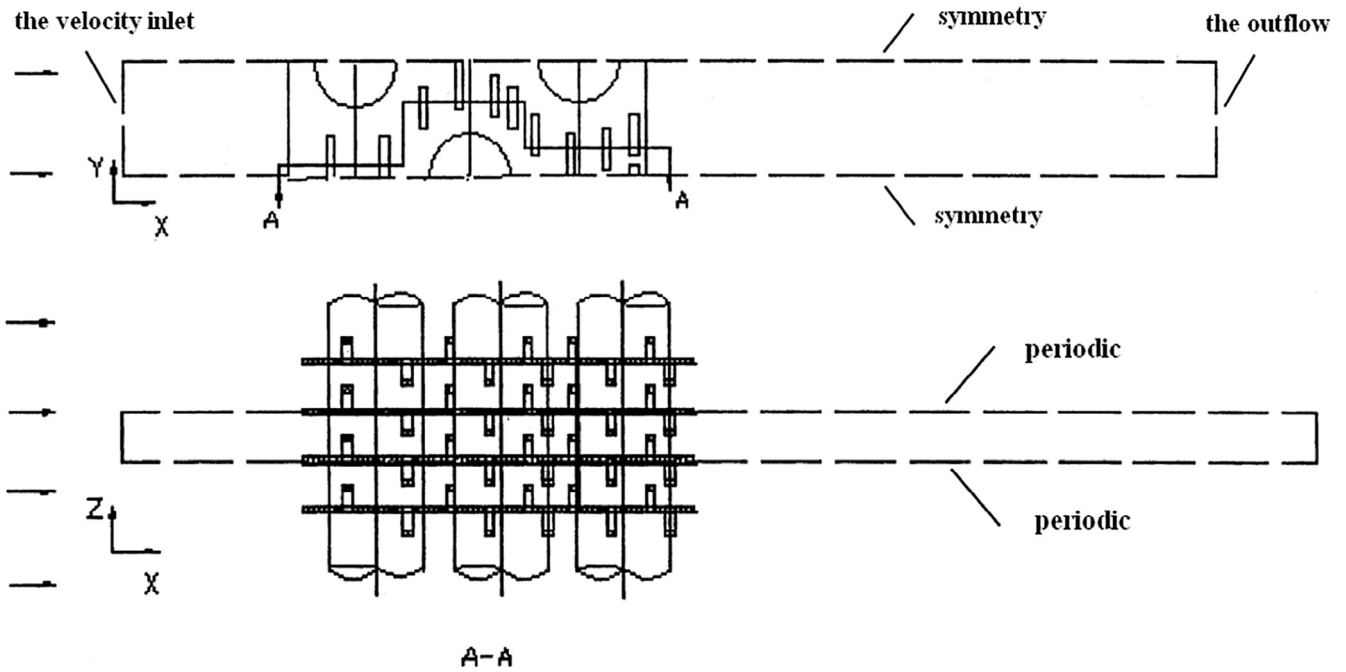


Fig. 3. Boundary conditions in the plain plate and slotted fins calculation region.

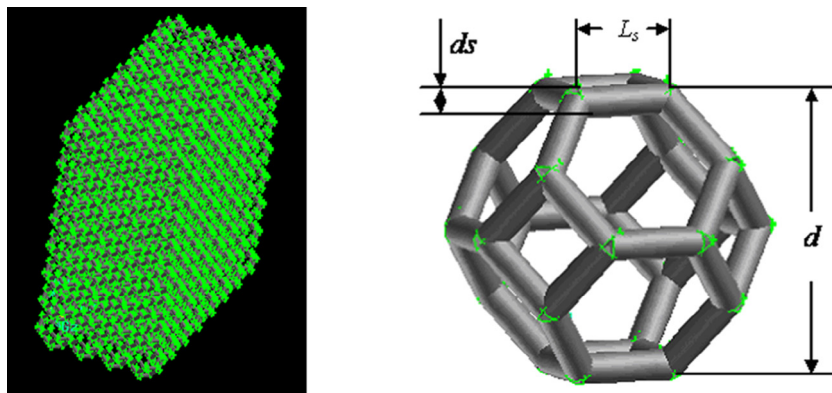


Fig. 4. Model of the tetrakaidecahedron unit.

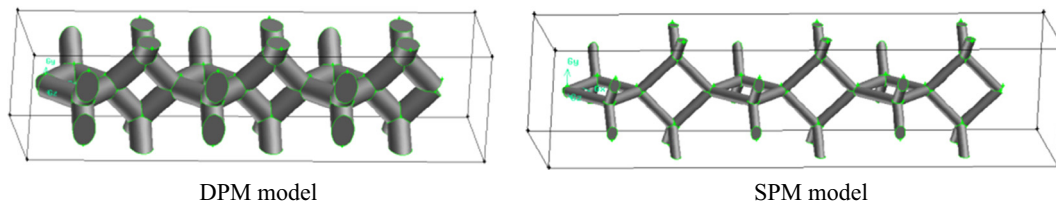


Fig. 5. DPM and SPM models of three periods.

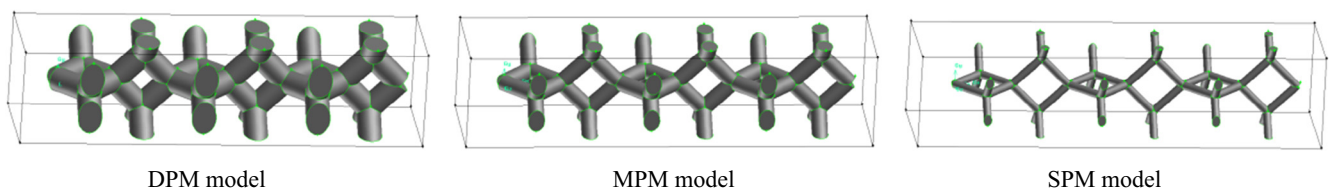


Fig. 6. DPM, MPM and SPM models with three periods.

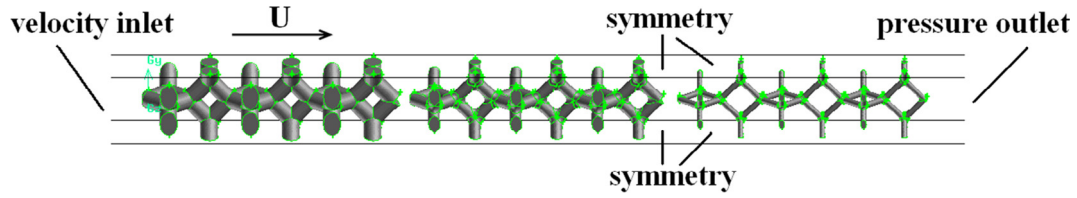


Fig. 7. Boundary conditions of D-M-S composite porous material.

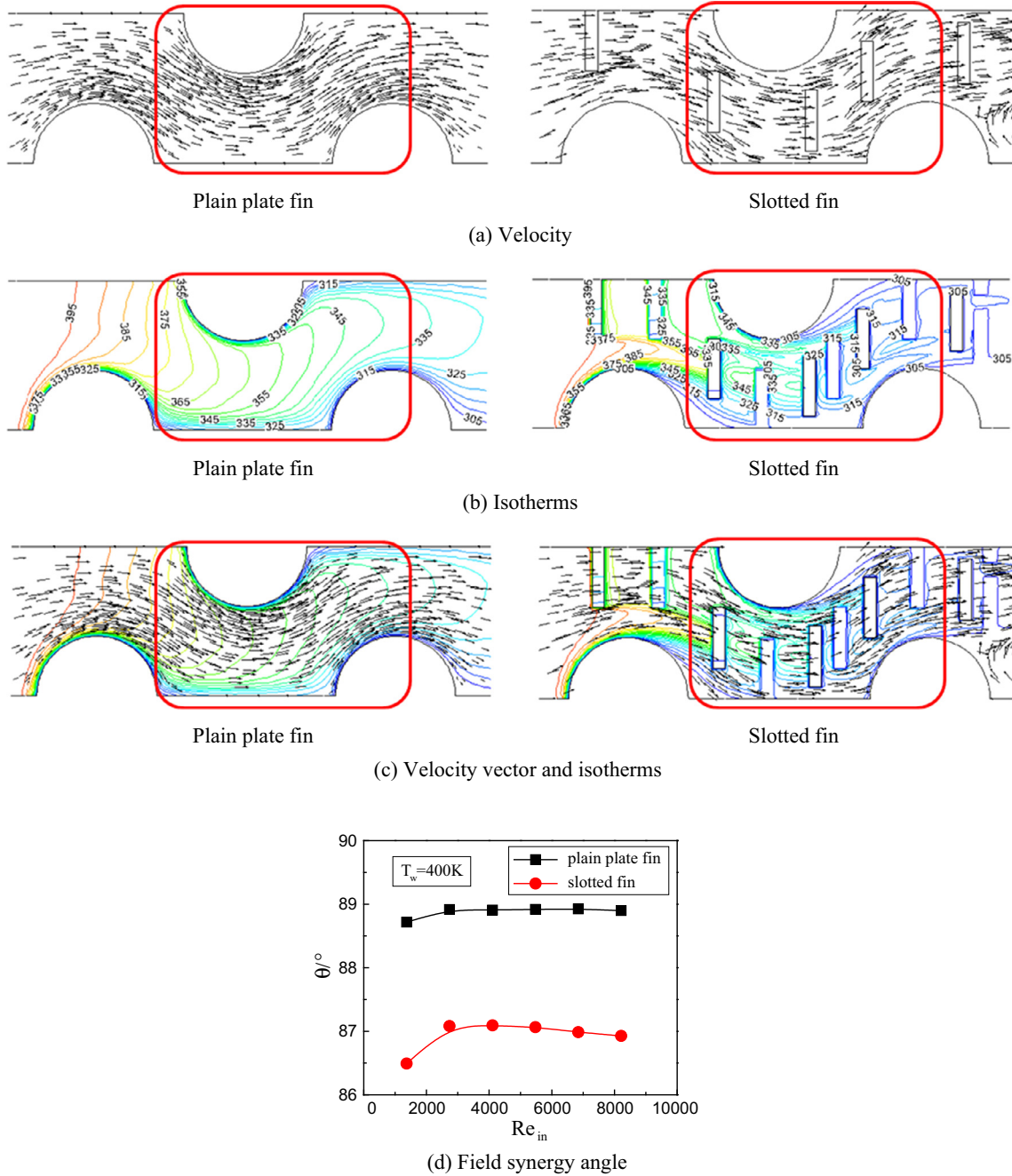


Fig. 8. Velocity, temperature fields and synergy angle of the plain plate and slotted fins.

are set as follows: the velocity and temperature of the flowing fluid are specified at the inlet boundary; while the pressure outlet boundary condition is set for the outlet; the symmetry boundary condition is adopted for the up, down, front and behind bound-

aries. For the surface of the porous material framework no slip and no jumping conditions should be satisfied. And its thermal boundary condition is given constant heat flux or constant wall temperature.

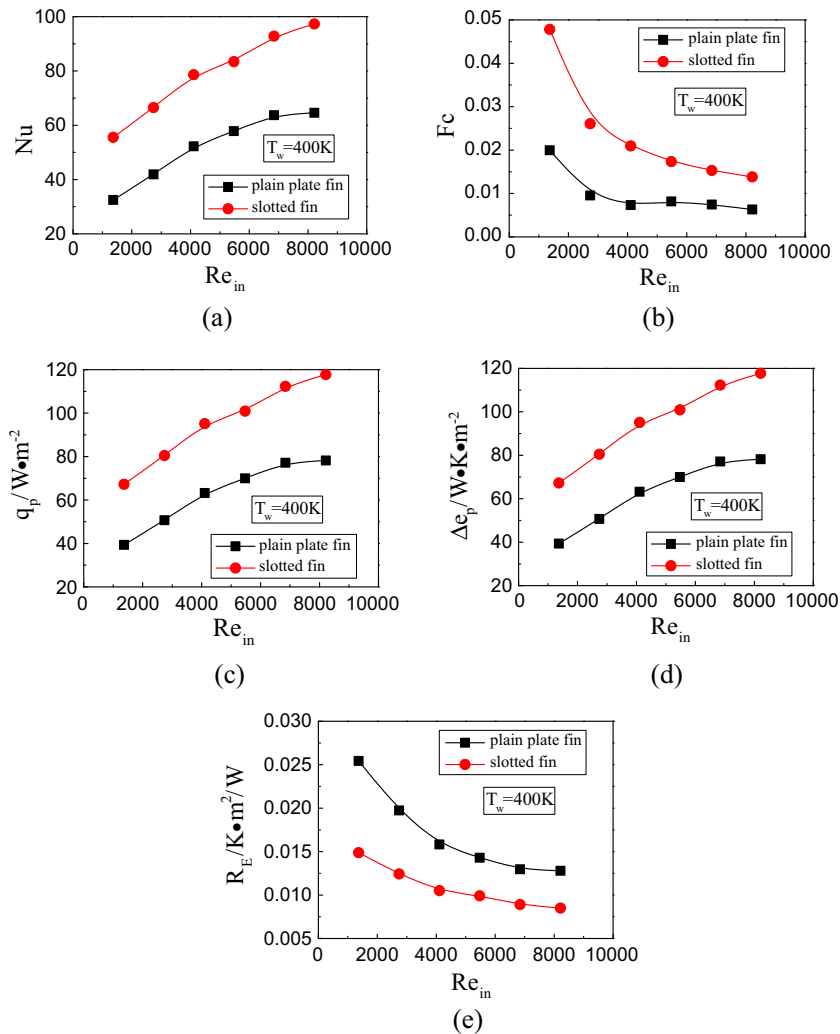


Fig. 9. Comparison of FSP and EDEP analyses for the plain plate and slotted fins given wall temperature.

In the simulation the computational region of the composite porous material is only the part occupied by air, i.e., the solid part is not included by given specified thermal boundary condition on its surface. The giving heat flux or temperature boundary condition of the porous material framework surface is set as the thermal boundary condition for the air-occupied regions.

When the air flows through the porous material interior, high turbulence intensity is developed and its value can be up to 60–80% [45]. The  $Re_{in}$  based on the equivalent diameter of the tetrakaidecahedron unit is about 100–1100. According to [46,47], the air flow state is turbulent. Menter et al. [47] predicted the heat transfer coefficient of such porous material through the SST  $k-\omega$  turbulent model and obtained satisfactory results. Hence, in this paper, the SST  $k-\omega$  turbulent model is employed.

The calculation domain is discretized by the tetrahedron elements and non-uniform grid system is used. The air physical properties are changed with the air temperature. The convection terms are discretized by the second-order upwind scheme [48]. The SIMPLE algorithm for coupling pressure and velocity is adopted [48,49].

#### 4. Numerical results and discussion

In this section numerical results will be presented. For each type of configuration the flow and temperature fields will be first presented, and followed by the discussion on the relationship between FSP and EDEP.

##### 4.1. Plain plate fin and slotted fin

When  $T_w = 400$  K and  $Re_{in} = 1369$ , the velocity field, temperature field and field synergy angle of the plain plate and slotted fins are shown in Fig. 8. It is to be noted that if the angle between velocity vector and temperature isotherm is bigger, the angle between velocity vector and temperature gradient is smaller. Then the synergy between velocity vector and temperature gradient is better, that means the heat transfer performance is improved.

In Fig. 8, we can find the synergy between velocity vector and temperature gradient is improved through cracking the fin. For example, in the region of the plain plate and slotted fins labeled by the red solid line, the averaged synergy angle is  $88.7^\circ$  from numerical data in the plain plate fin, while it is  $86.5^\circ$  for the slotted fin. This means that the heat transfer in this region is enhanced for the slotted fin.

The numerically predicted variations of  $Nu$  and field synergy number  $F_c$  with the inlet  $Re_{in}$  number are shown in Fig. 9. It can be seen that the slotted fin has both higher Nusselt number and field synergy number than those of the plain plate fin. The two results are consistent. Fig. 9 shows that the value range of field synergy number is 0–0.05, and it is much less than 1. So, there is a great room to improve the heat transfer performance of the plain plate and slotted fins.

The variation characteristics of field synergy number, heat transfer heat flux, entransy flux dissipation, equivalent weighted

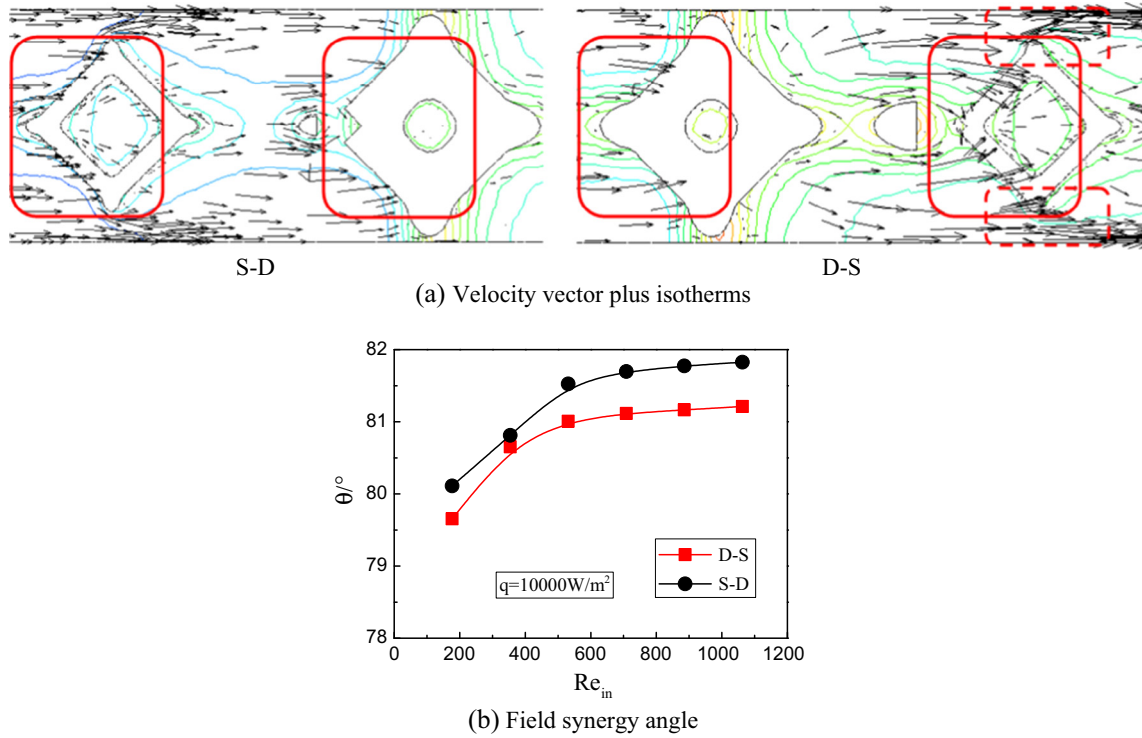


Fig. 10. Velocity, temperature fields and synergy angle of two composite porous materials.

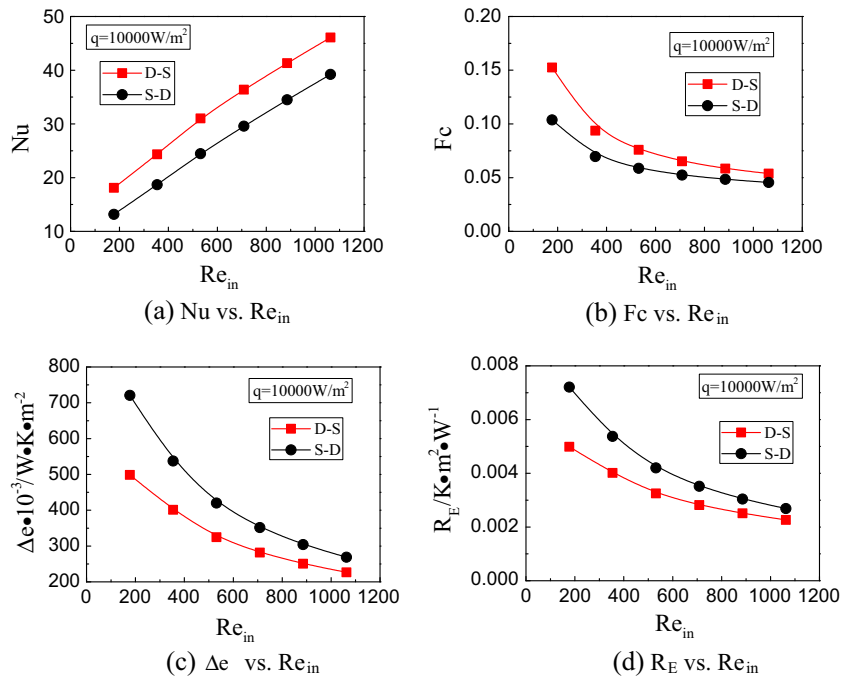


Fig. 11. FSP and EDEP analyses for the two composite porous materials with given heat flux.

thermal resistance of heat transfer with the inlet  $Re_{in}$  are shown in Fig. 9. From Fig. 9 the interrelationship between FSP and EDEP can be clearly observed, i.e., within the entire Reynolds number range studied, the heat transfer of slotted fin is better than that of the plain plate fin (Fig.9(b) and (c)). Correspondently the entransy dissipation of the slotted fin is larger than the plain plate fin (Fig.9(d) for given surface temperature case), while the thermal resistance of the slotted fin is less than the plain plate fin (Fig.9(e)).

#### 4.2. Type 1 porous material

When  $q = 10,000 \text{ W/m}^2$  and  $Re_{in} = 177$ , the velocity field, temperature field and field synergy angle of S-D and D-S composite porous materials are shown in Fig. 10. Through these figures, we can find that the synergy between velocity vector and temperature gradient in the D-S is better than that in the S-D (with the averaged synergy angle of the labeled region of S-D and D-S being  $80.1^\circ$  and

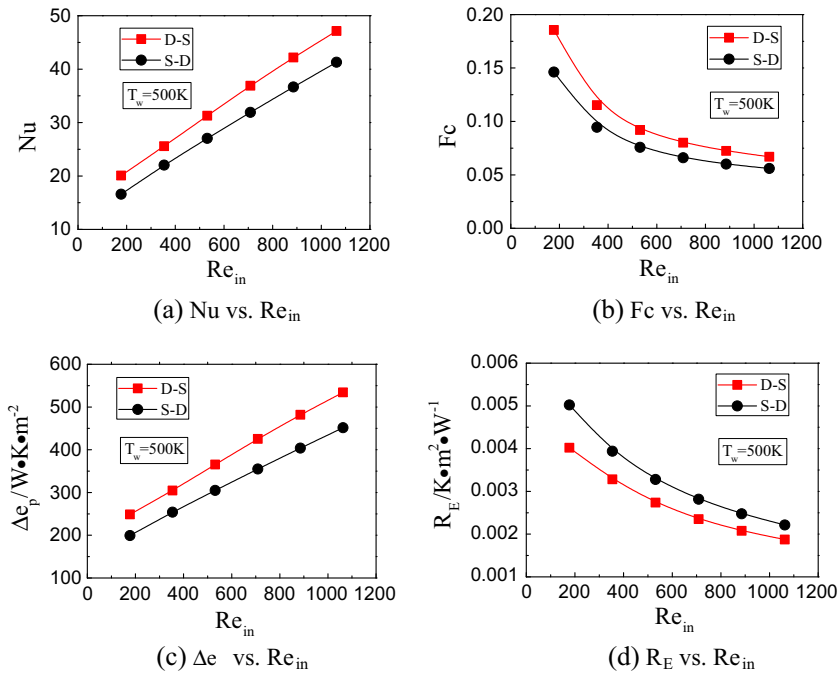


Fig. 12. FSP and EDEP analyses for two composite porous materials with given wall temperature.

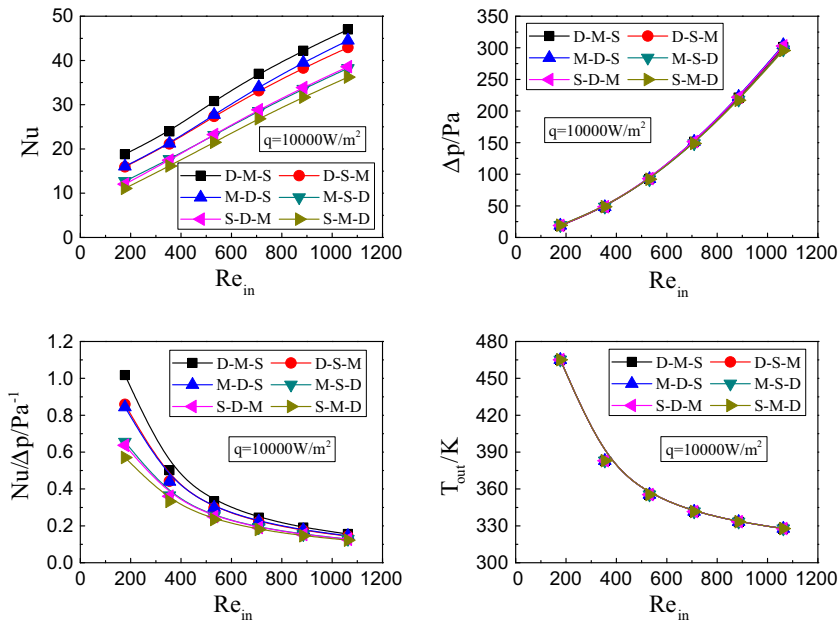


Fig. 13. Flow and heat transfer features of six composite porous materials at given heat flux.

79.6°, respectively). That is to say the heat transfer in the D-S is stronger than that in the S-D.

In the following the numerical results are analyzed by the FSP and EDEP to show the heat transfer performance of the two materials. First the results for given heat flux condition ( $q = 10,000 \text{ W/m}^2$ ) are presented in Fig. 11. From Fig. 11, we can find that when the thermal boundary condition is the given heat flux, the  $Nu$  of D-S is larger than that of S-D. And the sequence of the field synergy number  $Fc$  is: D-S > S-D. The orders of Nusselt number and field synergy number are consistent.

When the given thermal boundary condition is constant heat flux, from the MinEDP the best heat transfer case should have min-

imum entransy dissipation and minimum equivalent weighted thermal resistance. The results shown in Fig. 11 are consistent with this conclusion: the field synergy number  $Fc$  is: D-S > S-D. The entransy flux dissipation  $\Delta e$  has its sequence as: D-S < S-D. And the equivalent weighted thermal resistance  $R_E$  is: D-S < S-D.

Now the results for given wall temperature ( $T_w = 500 \text{ K}$ ) are discussed. The numerical calculation results are shown in Fig. 12. In Fig. 12 the sequence of Nusselt number and the field synergy number are both: D-S > S-D.

For the boundary condition of given wall temperature, EDEP says the entransy dissipation for the best heat transfer case should be the maximum. The results shown in Fig. 12 are totally agreeable

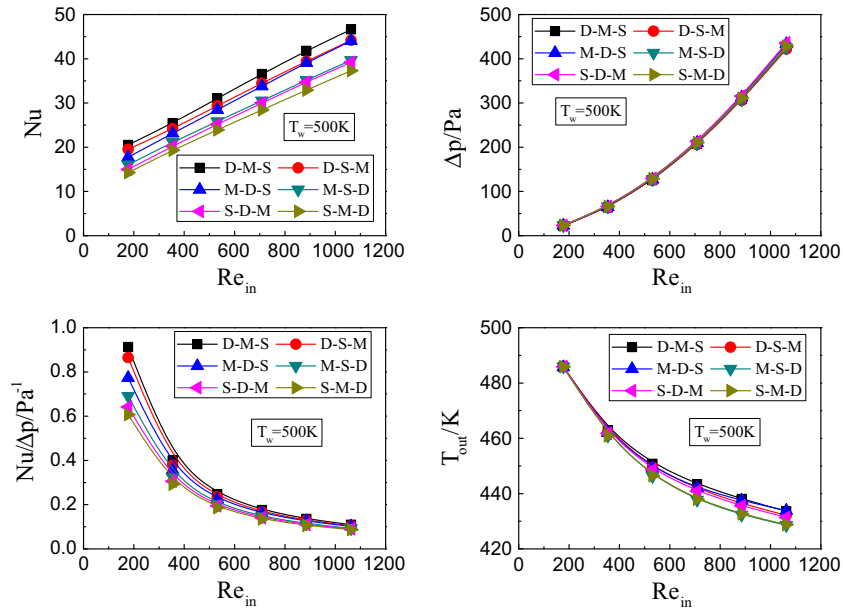


Fig. 14. Flow and heat transfer features of six composite porous materials at given wall temperature.

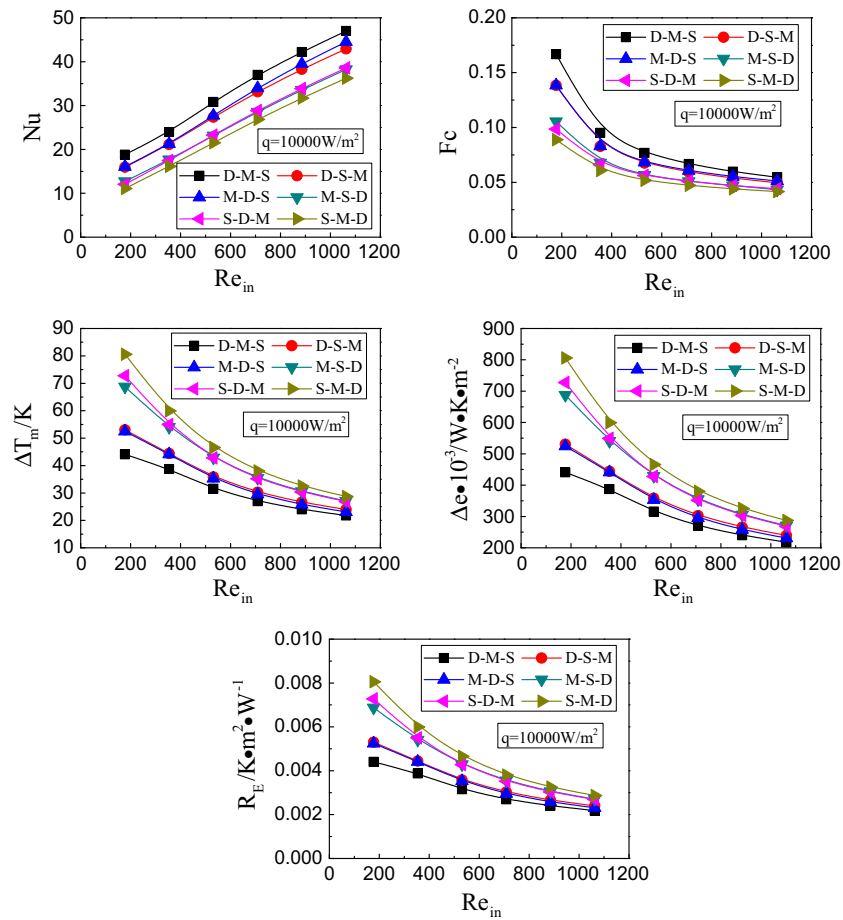


Fig. 15. FSP and EDEP analyses for six composite porous materials at given heat flux.

with this conclusion: Fig.12(c), (d) show that the entransy dissipation of D-S is larger than S-D, while the thermal resistance of D-S is less than S-D.

In conclusion, when heat transfer performance of the two porous materials (D-S vs. S-D) are compared either for given heat flux or for given wall temperature condition, the order obtained by FSP

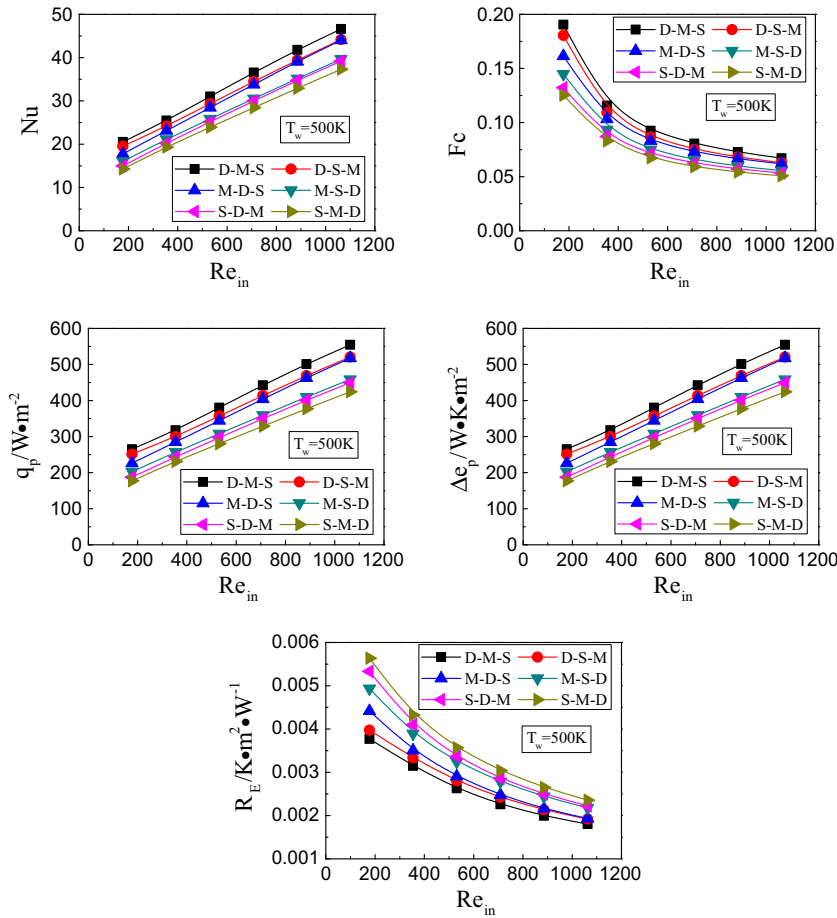


Fig. 16. FSP and EDEP analyses for six composite porous materials at given wall temperature.

via  $F_c$  is fully consistent with that obtained from EDEP, indicating that the two theories having their inherent consistency.

#### 4.3. Type 2 composite porous material

In this section the numerical results of the six composite porous materials are presented and analyzed.

##### 4.3.1. Fluid flow and heat transfer characteristics

###### 1. For given heat flux boundary condition

The predicted variation characteristics of  $Nu$ , pressure drop  $\Delta p$ ,  $Nu/\Delta p$  and air outlet temperature  $T_{out}$  with the inlet  $Re_{in}$  for the case of heat flux = 10,000 W/m<sup>2</sup> are shown in Fig. 13. From Fig. 13 we can obtain that: the pressure drops of six composite porous materials are almost the same. This is because for the six components the three elements are the same, and the difference is only in their orders. The outlet air temperatures of the six composite porous materials are the same because of the given constant heat flux boundary condition. However, the heat transfer performance of the D-M-S is the best and the one of the S-M-D is the worst.

###### 2. For given wall temperature boundary condition

The variation characteristics predicted for  $T_w = 500$  K are presented in Fig. 14. It can be seen that for the given wall temperature condition the D-M-S has the best heat transfer performance and the S-M-D is the worst.

In conclusion, for both given heat flux and wall temperature boundary conditions, the heat transfer performance of D-M-S is the best in the six composite porous materials.

##### 4.3.2. Analyses from FSP and EDEP

###### 1. For given constant heat flux

For given constant heat flux of solid framework of  $q = 10,000$  W/m<sup>2</sup>, the varying tendencies of  $Nu$  and field synergy number  $F_c$  with the inlet  $Re_{in}$  are shown in Fig. 15. From Fig. 15, the  $Nu$  increases with the inlet  $Re_{in}$ , and it is the biggest in the D-M-S and the smallest in the S-M-D. The field synergy number  $F_c$  is 0.05–0.17 for the six composite porous materials and it decreases with the inlet  $Re_{in}$ . The field synergy number  $F_c$  is the biggest in the D-M-S and the smallest in the S-M-D.

The variations of field synergy number, heat transfer temperature difference, entransy flux dissipation, equivalent weighted thermal resistance with the inlet Reynolds number are shown in Fig. 15. For given heat flux condition, from the FSP, the stronger the heat transfer, the bigger the field synergy number and the smaller the heat transfer temperature difference. From the MinEDP, the stronger the heat transfer, the smaller the entransy flux dissipation and the smaller the equivalent weighted thermal resistance. From Fig. 15, the results of these evaluation indicators agree with each other very well. So, for given heat flux boundary condition, the results evaluated from FSP via  $F_c$  and EDEP are consistent.

## 2. For given constant wall temperature

Fig. 16 shows the predicted variations of  $Nu$  and field synergy number with the inlet  $Re_{in}$  for  $T_w = 500$  K. From Fig. 16 it can be seen that for both Nusselt number and  $F_c$  the D-M-S is the biggest and S-M-D is the smallest. The values of  $F_c$  is 0.06–0.20 for the given constant wall temperature condition.

In Fig. 16 the results analyzed from the FSP and EDEP are presented. For given wall temperature condition, from the FSP the better the heat transfer performance the bigger the field synergy number and the bigger the heat flux. From the MaxEDP, the bigger the heat transfer heat flux the larger the entransy flux dissipation and the smaller the equivalent weighted thermal resistance. The curves shown in Fig. 16 are totally agreeable with the above statements: for the field synergy number, the biggest one is in the D-M-S and the smallest one is in the S-M-D. For the entransy flux dissipation the biggest one is in the D-M-S and the smallest one is in the S-M-D. The equivalent weighted thermal resistance has its biggest one in the S-M-D and its smallest one in the D-M-S.

## 5. Conclusions

In this paper, the field synergy number is adopted to analyze the synergy between velocity vector and temperature gradient for the entire domain. For a number of situations, including the plain plate fin, slotted fin and composite porous materials, flows of laminar and turbulent, thermophysical properties of constant and variable, and thermal boundary conditions of constant heat flux and constant wall temperature, the analyzed results from the FSP via  $F_c$  are totally consistent with the results analyzed by the EDEP. Thus the inherent connection and consistency between FSP via  $F_c$  and EDEP is once again revealed. Such consistency between the FSP and the entransy theory can be regarded as a kind of demonstration of the reliability and correctness of both the FSP and the entransy theory.

## Acknowledgements

This work is supported by the Foundation of Innovative Research Group of the National Natural Science Foundation of China (51721004), the National Key Basic Research Program of China (973 Program) (2013CB228304) and the 111 Project (B16038).

## Conflict of interest

We declare that we have no financial and personal relationships with other people or organizations that can inappropriately influence our work; there is no professional or other personal interest of any nature or kind in any product, service and/or company that could be construed as influencing the position presented in, or the review of, the manuscript entitled, “Study on the Consistency between Field Synergy Principle and Entransy Dissipation Extremum Principle”.

## References

- W.Q. Tao, Z.Y. Guo, B.X. Wang, Field synergy principle for enhancing convective heat transfer—its extension and numerical verifications, *Int. J. Heat Mass Transf.* 45 (18) (2002) 3849–3856.
- Z.Y. Guo, D.Y. Li, B.X. Wang, A novel concept for convective heat transfer enhancement, *Int. J. Heat Mass Transf.* 41 (14) (1998) 2221–2225.
- Z.Y. Guo, Mechanism and control of convective heat transfer – coordination of velocity and heat flow fields, *Chinese Sci. Bull.* 46 (7) (2001) 596–599.
- Z.Y. Guo, W.Q. Tao, R.K. Shah, The field synergy (coordination) principle and its applications in enhancing single phase convective heat transfer, *Int. J. Heat Mass Transf.* 48 (9) (2005) 1797–1807.
- Z.X. Li, Z.Y. Guo, *Optimization Principles for Heat Convection*, Springer-Verlag, Berlin Heidelberg, 2011.
- T.S. Zhao, Y.J. Song, Forced convection in a porous medium heated by a permeable wall perpendicular to flow direction: analyses and measurements, *Int. J. Heat Mass Transf.* 44 (5) (2001) 1031–1037.
- W.Q. Tao, Y.L. He, Q.W. Wang, Z.G. Qu, F.Q. Song, A unified analysis on enhancing single phase convective heat transfer with field synergy principle, *Int. J. Heat Mass Transf.* 45 (24) (2002) 4871–4879.
- L.D. Ma, Z.Y. Li, W.Q. Tao, Experimental verification of the field synergy principle, *Int. Commun. Heat Mass* 34 (3) (2007) 269–276.
- M. Zeng, W.Q. Tao, Numerical verification of the field synergy principle for turbulent flow, *J. Enhanc. Heat Transf.* 11 (4) (2004) 453–460.
- S. Shen, W. Liu, W.Q. Tao, Analysis of field synergy on natural convective heat transfer in porous media, *Int. Commun. Heat Mass* 30 (8) (2003) 1081–1090.
- C.K. Chen, T.S. Yen, Y.T. Yang, Lattice Boltzmann method simulation of backward-facing step on convective heat transfer with field synergy principle, *Int. J. Heat Mass Transf.* 49 (5–6) (2006) 1195–1204.
- R.X. Cai, C.H. Gou, Discussion on the convective heat transfer and field synergy principle, *Int. J. Heat Mass Transf.* 50 (25–26) (2007) 5168–5176.
- J.M. Wu, W.Q. Tao, Investigation on laminar convection heat transfer in fin-and-tube heat exchanger in aligned arrangement with longitudinal vortex generator from the viewpoint of field synergy principle, *Appl. Therm. Eng.* 27 (14–15) (2007) 2609–2617.
- Z.G. Qu, W.Q. Tao, Y.L. He, Three-dimensional numerical simulation on laminar heat transfer and fluid flow characteristics of strip fin surface with X-arrangement of strips, *J. Heat Transfer* 126 (5) (2004) 697–707.
- W.Q. Tao, Y.L. He, Z.G. Qu, Y.P. Cheng, Application of the field synergy principle in developing new type heat transfer enhanced surfaces, *J. Enhanc. Heat Transf.* 11 (4) (2004) 435–452.
- W.L. Chen, Z. Guo, C.O.K. Chen, A numerical study on the flow over a novel tube for heat-transfer enhancement with a linear Eddy-viscosity model, *Int. J. Heat Mass Transf.* 47 (14–16) (2004) 3431–3439.
- Y.P. Cheng, Z.G. Qu, W.Q. Tao, Y.L. He, Numerical design of efficient slotted fin surface based on the field synergy principle, *Numerical Heat Transfer Applications* 45 (6) (2004) 517–538.
- J.A. Meng, X.G. Liang, Z.X. Li, Z.Y. Guo, Numerical study on low Reynolds number convection in alternate elliptical axis tube, *J. Enhanc. Heat Transf.* 11 (4) (2004) 307–314.
- J.A. Meng, X.G. Liang, Z.X. Li, Field synergy optimization and enhanced heat transfer by multi-longitudinal vortexes flow in tube, *Int. J. Heat Mass Transf.* 48 (16) (2005) 3331–3337.
- Y.L. He, W.Q. Tao, F.Q. Song, W. Zhang, Three-dimensional numerical study of heat transfer characteristics of plain plate fin-and-tube heat exchangers from view point of field synergy principle, *Int. J. Heat Fluid Flow* 26 (3) (2005) 459–473.
- Q. Chen, J.X. Ren, Z.Y. Guo, Fluid flow field synergy principle and its application to drag reduction, *Chinese Sci. Bull.* 53 (11) (2008) 1768–1772.
- Y.P. Cheng, T.S. Lee, H.T. Low, Numerical simulation of conjugate heat transfer in electronic cooling and analysis based on field synergy principle, *Appl. Therm. Eng.* 28 (14–15) (2008) 1826–1833.
- J.K. Kuo, T.S. Yen, C.O.K. Chen, Improvement of performance of gas flow channel in PEM fuel cells, *Energy Convers. Manage.* 49 (10) (2008) 2776–2787.
- Z.Y. Guo, H.Y. Zhu, X.G. Liang, Entransy—A physical quantity describing heat transfer ability, *Int. J. Heat Mass Transf.* 50 (13–14) (2007) 2545–2556.
- Q. Chen, J.X. Ren, Generalized thermal resistance for convective heat transfer and its relation to entransy dissipation, *Chinese Sci. Bull.* 53 (23) (2008) 3753–3761.
- Q. Chen, M. Wang, N. Pan, Z.Y. Guo, Optimization principles for convective heat transfer, *Energy* 34 (9) (2009) 1199–1206.
- Z.Y. Guo, X.B. Liu, W.Q. Tao, R.K. Shah, Effectiveness–thermal resistance method for heat exchanger design and analysis, *Int. J. Heat Mass Transf.* 53 (13–14) (2010) 2877–2884.
- X.B. Liu, M. Wang, J.A. Meng, E. Ben-Naim, Z.Y. Guo, Minimum entransy dissipation principle for optimization of transport networks, *Int. J. Nonlin. Sci. Numer. Simul.* 11 (2) (2010) 113–120.
- Q. Chen, N. Pan, Z.Y. Guo, A new approach to analysis and optimization of evaporative cooling system II: Applications, *Energy* 36 (5) (2011) 2890–2898.
- J. Wu, X.T. Cheng, Generalized thermal resistance and its application to thermal radiation based on entransy theory, *Int. J. Heat Mass Transf.* 58 (1–2) (2013) 374–381.
- B. Zhou, X.T. Cheng, X.G. Liang, Power and heat-work conversion efficiency analyses for the irreversible Carnot engines by entransy and entropy, *J. Appl. Phys.* 113 (12) (2013) 124904.
- Y.D. Zhu, Z. Hu, Y.D. Zhou, J. Liang, L.J. Yu, Applicability of entropy, entransy and exergy analyses to the optimization of the organic Rankine cycle, *Energy Convers. Manage.* 88 (2014) 267–276.
- K.H. Kim, K.J. Kim, Comparative analyses of energy–exergy–entransy for the optimization of heat-work conversion in power generation systems, *Int. J. Heat Mass Transf.* 84 (4) (2015) 80–90.
- Y. Han, D.B. Wang, C.C. Zhang, Y.J. Zhu, The entransy degeneration and entransy loss equations for the generalized irreversible Carnot engine system, *Int. J. Heat Mass Transf.* 106 (2016) 895–907.
- Q. Chen, X.G. Liang, Z.Y. Guo, Entransy theory for the optimization of heat transfer – A review and update, *Int. J. Heat Mass Transf.* 63 (15) (2013) 65–81.
- X.T. Cheng, X.G. Liang, Entransy, entransy dissipation and entransy loss for analyses of heat transfer and heat-work conversion processes, *J. Therm. Sci. Technol.* 8 (2) (2013) 337–352.

- [37] X.T. Cheng, X.G. Liang, Entransy: its physical basis, applications and limitations, *Chinese Sci. Bull.* 59 (36) (2014) 5309–5323.
- [38] Y.L. He, W.Q. Tao, Chapter three – convective heat transfer enhancement: mechanisms, techniques, and performance evaluation, *Adv. Heat Transf.* 46 (2014) 87–186.
- [39] L.G. Chen, Progress in entransy theory and its applications, *Chinese Sci. Bull.* 57 (34) (2012) 4404–4426.
- [40] L.G. Chen, Progress in optimization of mass transfer processes based on mass entransy dissipation extremum principle, *Sci. China: Technol. Sci.* 57 (12) (2014) 2305–2327.
- [41] T. Zhang, X.H. Liu, H.D. Tang, J. Liu, Progress of entransy analysis on the air-conditioning system in buildings, *Sci. China: Technol. Sci.* 59 (10) (2016) 1–12.
- [42] F. Yuan, Q. Chen, Two energy conservation principles in convective heat transfer optimization, *Energy* 36 (9) (2011) 5476–5485.
- [43] Y.L. He, W.Q. Tao, Numerical studies on the inherent interrelationship between field synergy principle and entransy dissipation extreme principle for enhancing convective heat transfer, *Int. J. Heat Mass Transf.* 74 (74) (2014) 196–205.
- [44] Z.Q. Yu, Y.L. Feng, W.J. Zhou, Y. Jin, M.J. Li, Z.Y. Li, W.Q. Tao, Study on flow and heat transfer characteristics of composite porous material and its performance analysis by FSP and EDEP, *Appl. Energy* 112 (4) (2013) 1367–1375.
- [45] M.J. Hall, J.P. Hiatt, Measurements of pore scale flows within and exiting ceramic foams, *Exp. Fluids* 20 (6) (1996) 433–440.
- [46] M. Kaviany, *Principles of Heat Transfer in Porous Media*, second ed., Springer Press, New York, 1995.
- [47] F.R. Menter, M. Kuntz, R. Langtry, Ten years of industrial experience with the SST turbulence model, *Heat Mass Transf.* 4 (2003) 625–632.
- [48] W.Q. Tao, *Numerical Heat Transfer*, second ed., Xi'an Jiaotong University Press, Xi'an, 2001.
- [49] S.V. Patankar, *Numerical Heat Transfer and Fluid Flow*, Hemisphere Press, New York, 1980.